CHRACTERIZED SOURCE MODEL OF THE 2017 MW6.5 JIUZHAIGOU EARTHQUAKE

H. Wu[1,2], K. Irikura[3], S. Kurahashi[4]

[1] Fengming Road 1000, Licheng District, Jinan, 250014, Shandong province, China, School of Civil Engineering, Shandong Jianzhu University, wh_ce@sdjzu.edu.cn
[2] Fengming Road 1000, Licheng District, Jinan, 250014, Shandong province, China, Key Laboratory of Building Structural Retrofitting and Underground Space Engineering (Shandong Jianzhu University), Ministry of Education.
[3] Yachigusa 1247, Yakusa, Toyota, 4700392, Aichi Prefecture, Japan, Disaster Prevention Research Center, Aichi Institute of Technology, irikuar@geor.or.jp
[4] Yachigusa 1247, Yakusa, Toyota, 4700392, Aichi Prefecture, Japan, Department of Civil Engineering, Aichi Institute of Technology, susumu@aitech.ac.jp

Abstract

We construct the characterized source model during the 2017 M_w6.5 Jiuzhaigou earthquake occurring on Aug. 8, 2017 in Jiuzhaigou county, Sichuan province, China. This model can synthesize the ground motions of the mainshock in the period range of 0.05s~5.0s within the engineering interests which is important for understanding the relationship between the ground motion characteristics and the damage of buildings. The characterized source model estimated by the empirical Green's function method (EGFM) is composed of one strong motion generation area (SMGA) inside the mainshock fault plane. We regard the ground motions of an M_w4.7 aftershock observed at three near-source strong-motion stations (i.e. 051JZB, 051JZW, and 051JZY) to be the EGFs of which the hypocenter is near the large slips areas of the mainshock and the source mechanism is similar to the mainshock. We estimate the fault size of the EGF event (1.46km in length and width) from the corner frequency of the source spectral ratio of the mainshock to the EGF event, and determine other parameters by simulated annealing algorithm, including the stress parameter ratio C=1.54 and a parameter related to number of summation N=6, rupture velocity V_r=2.7km/s, rise time of the mainshock T=0.6s, and the position of the rupture starting point inside the SMGA. The area, stress parameter and seismic moment of the SMGA are 76.7km^2, 16.8MPa and 4.6×10^{18}N·m, respectively. We confirm that the synthesized ground motions are in reasonably good agreement with the observed ground motions in the period range of 0.05s~5.0s within the engineering interests at three strong-motion stations. The relationships between the SMGA and the seismic moment and between the amplitude of acceleration source spectrum in the short period range and the seismic moment for the 2017 M_w6.5 Jiuzhaigou earthquake, the 2013 M_w6.1 Ludian earthquake, and the 2008 M_w7.9 Wenchuan earthquake agree well with the conventional scaling relationships. It suggests that the conventional scaling relationships are applicable for the prediction of ground motions in the future crustal earthquakes in China.

Keywords: characterized source model, the 2017 Mw6.5 Jiuzhaigou earthquake, empirical Green's function

1. Introduction

The 2017 M_w6.5 Jiuzhaigou earthquake struck the Jiuzhaigou county, Sichuan province, China on Aug. 8, 2017. This is another moderate earthquake after the 2013 M_w6.6 Lushan earthquake which occurred on Apr. 20, 2013 in Sichuan province. The ground motions were observed at as many as 66 strong-motion stations during the mainshock, three of which were less than 40 km apart from the hypocenter. The largest PGA was 185 gal observed at the station-051JZB closest to the epicenter. The strong ground motions of the mainshock caused 25 people dead, 6 people missing and 525 people injured as reported at 20:00 local time on Aug. 13, 2017, brought about much damage to buildings and lifelines [1], and triggered geological hazards, such as landslides and debris flows, which even destroyed several world heritage sites including Sparking lake and Nuorilang waterfall [2]. The mainshock ruptured an unknown blind strike-slip fault which might be the northern extension of the Huya fault between the Tazang fault and the Minjiang fault [3,4,5]. It became quite urgent to study the source model in such fault for prediction of ground motions in future earthquakes.

Several kinematic source models have been presented by some researchers to study the rupture process of the mainshock. These models can be estimated from coseismic deformation observed by GPS and InSAR [6], inversion of teleseimic data [7,8], joint inversion of teleseismic data and InSAR [9], or joint inversion of GNSS and teleseismic data [10]. Although these source models exhibit different fault sizes in length and width due to different data sources, the slip distributions are almost the same, e.g. the large slips distribute around the hypocenter. These kinematic source models are used to synthesize long-period (e.g. an order of ten seconds) ground motions, whereas stochastic source model is used to synthesize short-period (<1.0s) ground motions [11]. In this study, we aim to establish the characterized source model that is capable of synthesizing ground motions in the period of engineering interests (e.g. 0.05s~20.0s). Then we investigate whether the relationships between source parameters and seismic moment agree with the conventional scaling relationships. The conclusion of this study is expected to be helpful in the study of prediction of ground motions in future crustal earthquakes in China as long as the parameters such as entire fault area and SMGA are estimated from the conventional scaling relationships.

2. Methodology

As there are many ground motions of small events, such as foreshocks and aftershocks, we can always select out ground motions of some small events to be the empirical Green's functions (EGF). Therefore, we apply the empirical Green's function method (EGFM) to establish the characterized source model. This method was firstly proposed by [12] and then revised by [13] and [14,15]. Irikura [15,16] expressed the ground motions of large event as a superposition of the ground motions of small events in Eq. (1)~(3).

$$U(t) = \sum_{i=1}^{N}\sum_{j=1}^{N} \frac{r}{r_{ij}} F(t - t_{ij}) * (C \cdot u(t)) \tag{1}$$

$$t_{ij} = \frac{r_{ij} - r_o}{Vs} + \frac{\xi_{ij}}{V_r} \tag{2}$$

$$F(t) = \delta(t) + \frac{1}{n'(1-1/e)} \cdot \sum_{k=1}^{(N-1)n'} \left[\exp\left\{ \frac{-(k-1)}{(N-1)n'} \right\} \cdot \delta\left\{ t - \frac{(k-1)T}{(N-1)n'} \right\} \right] \tag{3}$$

Where U(t) and u(t) are ground motions of large event and small event which is regarded as the EGF event, respectively. The subscripts i and j are indices of subfaults increasing along the strike and dip directions, respectively. The terms r, r_{ij}, and r_0 are the respective distances from the station to the hypocenter of the small event, from the station to the (i,j) subfault, and from the station to the rupture starting point on the fault plane of the large event. The term ξ_{ij} is the distance between the rupture starting point and the (i,j) subfault. V_s and V_r are the shear-wave velocity near the source area and rupture velocity on the fault plane, respectively. F(t) is the correction function of slip velocity between large and small events which was modified by [16]. C and N are the ratios of stress parameters and fault sizes (length or width) between the large and small events, respectively. T is the rise time of large event, and n' is the division number to shift the artificial periodicity to a frequency higher than that of interests.

3. Parameters of the characterized source model

The characterized source model is featured by some strong motion generation areas (SMGAs) which are composed of a certain number of subfaults with large stress parameter, and a background area in the seismogenic zone on the fault plane. As the strong ground motions are mainly affected by the SMGAs where the large slips distribute, we suppose that strong motions from characterized source model are attributed to ground motions only from SMGAs. The number of SMGAs depends on the complexity of the source rupture process. The inversion results of several kinematic source models showed that the large slips distributed around the hypocenter, which implies that one SMGA inside the mainshock fault plane might be adequate for the characterized source model of this earthquake. We attempt to establish such characterized source model that the ground motions of the mainshock can be synthesized by Eq. (1) which sums the EGFs on the SMGA. We need to determine the following factors: the EGFs, SMGA's position inside the fault plane of the mainshock, position of rupture starting point inside the SMGA, fault size (length and width) of the EGF event, shear-wave velocity-V_s in the source area, proportion coefficients-C and N, rupture velocity-V_r, and rise time-T.

First, we select out the EGF event from some aftershocks, the ground motions of which were observed at the same stations as those of the mainshock. Fig. 1 shows the positions of kinematic source model [10], and distribution of epicenters of the mainshock and aftershocks, and strong-motion stations. The epicenters of aftershocks distribute along the strike direction. The aftershock can be regarded as the EGF event under some conditions, such as the hypocenter is near the SMGAs, and the source mechanism is similar to the mainshock. These conditions ensure that the EGF event shares the similar source, path and site effects with the mainshock. Table 1 lists the information, such as the position of hypocenter, magnitude, and strike/dip/rake, of the mainshock and an aftershock. It is evident that this aftershock satisfies the above conditions as an EGF event. The ground motions of the EGF event were observed at six strong-motion stations shown with crosses in Fig. 1, three of which, 051JZB, 051JZW, and 051JZY shown in squares, obtained the ground motions of the mainshock. The synthesis of ground motions during the mainshock are accomplished by use of the EGFs at these three strong-motion stations.

Second, we estimate the fault length and width of the EGF event from the corner frequency of the source spectral ratio of the mainshock to the EGF event [19]. We employ the S-wave part of the records of the mainshock and the EGF event to evaluate the Fourier spectra (vector summation of two horizontal components), and then obtain the source spectral ratios of the mainshock to the EGF event to remove the path and site effects. We show the individual source spectral ratios with gray curves at three strong-motion stations, and the geometrical average of the source spectral ratios with thick curves in Fig. 2. The amplitudes of source spectral ratios are small and the slopes are steep under 0.2 Hz, which might be caused by the small SN ratios of low-frequency ground motions. According to the omega-squared law, we can estimate some theoretical source spectral ratios when the maximum amplitude is kept to be M_o/m_o, and corner frequencies of the EGF (f_{ca}) and the mainshock (f_{cm}) are provided. Given the fitting frequency range between 0.2Hz and 20.0Hz, we obtain the best fitting of the theoretical source spectral ratio to the geometrical average one for f_{ca}=1.54Hz and f_{cm}=0.23Hz, as shown in Fig. 2. As the hypocenter is in the eastern Tibetan Plateau, the shear-wave velocity-V_s in the source region is 3.44 km/s according to Table S1 in the supplement of [20]. Thus, we obtain the fault size of the EGF event from the corner frequency by r=2.34V_s/(2πf_{ca})=0.83km [21,22], and consequently the stress parameter is Δσ=(7/16)(M_o/r^3)=10.9MPa [23]. For small or moderate earthquakes, we regard the fault length to be identical with the fault width, thus the fault length (or width) of the EGF is $\sqrt{\pi}r$=1.46km.

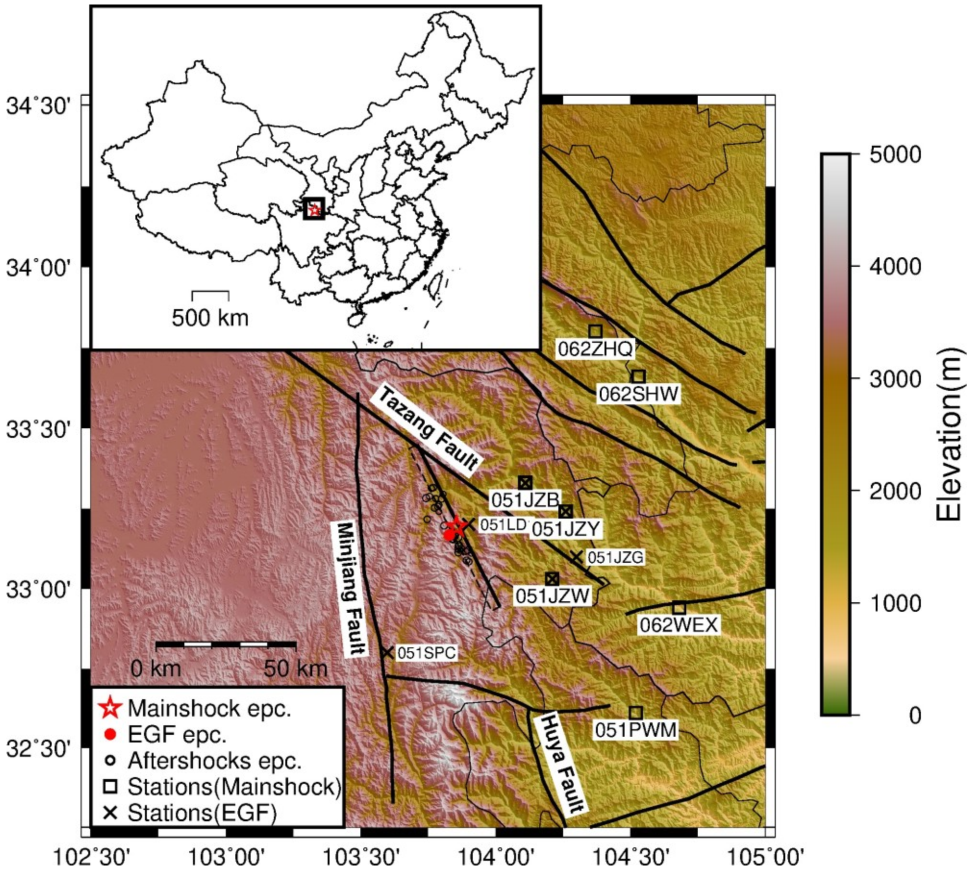

Fig. 1 – Map showing strong-motion stations, epicenters of the mainshock and the EGF event, and position of the kinematic source model [10]. Squares and crosses signify the positions of strong-motion stations of the mainshock and the EGF event, respectively. The thick lines show the fault traces [17].

Table 1 – Information of the mainshock (USGS) and the EGF event [18]

Origin time (Beijing time)	2017/08/08, 21:19	2017/08/10, 05:05
Latitude (deg.)	33.193	33.1671
Longitude (deg.)	103.855	103.8281
Depth (km)	9	10
Mw	6.5	4.7
Mo (N·m)	8.0×10^{18}	1.2×10^{16}
Strike/dip/rake (°)	153.0/84.0/-33.0	165.0/78.0/3.0

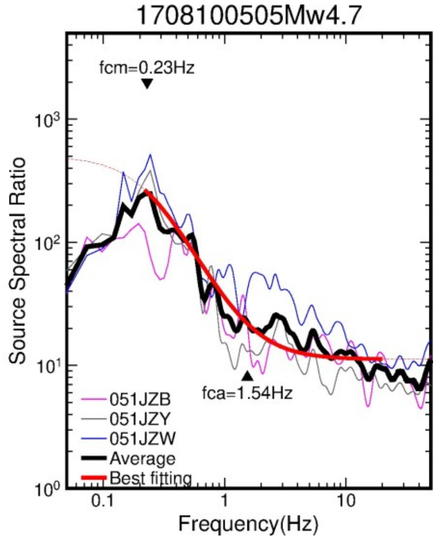

Fig. 2 – Source spectral ratios of ground motions of the mainshock to those of the EGF event. The thin curves are the source spectral ratios at three strong-motion stations, and the thick black curve is the geometrical average of those three source spectral ratios. The thick red curve is the theoretical source spectral ratio which is best fitting to the geometrical average of three source spectral ratios.

Table 2 – Parameters related to the characterized source model

C, N	1.54, 6
Indices of rupture starting point (i,j)	(1, 4)
Length, width (km)	8.76, 8.76
Rise time (s)	0.60
Rupture velocity (km/s)	2.70
Stress parameter (MPa)	16.8
Mo (N·m)	4.6×10^{18}

Third, we apply the simulated annealing algorithm to determine the remained parameters, i.e., V_r, T, C and N, and indices-(i,j) of rupture starting point, which are independent variables. We search the V_r in the range of (0.55~0.95)×V_s in the source region, rise time of the EGF event ranging from 0.02s to 0.50s, C ranging from 1 to 7, N ranging from 4 to 9, and indices of rupture starting point ranging from 1 to N along the strike and dip directions, respectively. The search intervals of these parameters except i and j are not constant value during the iterations, as they are evaluated from the generating temperature and uniform random values in each iteration [24]. Once the parameters are given, the ground motions of the mainshock is synthesized by Eq. (1) with the EGFs, and then compared with the observed ground motions. In a strict sense, Eq. (1) is formulated only for S-wave portions, but the P-wave converted from SV-wave near the stations are observed before the S-wave arrival, which is also applicable for Eq. (1) as the SV-P waves propagate at the S-wave velocity from the source to station. Therefore, we extract the waveforms of 25s long starting from 5s before the P-wave arrivals from the whole records of the EGF event and the mainshock, and then apply a bandpass filter of 0.20Hz~20.0Hz. We estimate the residuals from the acceleration envelopes and displacement waveforms of the synthesized and observed ground motions. As the indices of rupture starting point sequentially change from 1 to N in each iteration, the smallest residual is regarded to be the misfit function for the current iteration. The simulated annealing algorithm tends to search many local minima when the temperature is high at the beginning and gradually converges to a global minimum as the temperature decreases. We finally obtain the parameters as listed in Table 2 of the characterized source model for synthesizing ground motions when the misfit function reaches the global minimum after all the iterations are finished.

4. Results of the synthesized ground motions

We obtain a best-fit characterized source model of this earthquake consisting of one SMGA which is near the large slips area as shown in Fig. 3. The SMGA is composed of 6 subfaults along the strike direction with a length of 8.76km, and 6 subfaults along the dip direction with a width of 8.76km. Fig. 4 shows the waveforms of acceleration, velocity and displacement in the NS and EW components of the synthesized and observed ground motions at three strong-motion stations. Fig. 5 shows the comparisons of Fourier spectra between the synthesized and observed ground motions. Fig. 6 shows the comparisons of pseudo-velocity response spectra (vector summation in two horizontal components) with a damping ratio h=5% between the synthesized and observed ground motions. On the one hand, we confirm that the synthesized waveforms are in reasonably good agreement with the observed waveforms, and the shape and amplitude of pseudo-velocity response spectra of the synthesized ground motions are almost consistent with those of the observed ground motions. On the other hand, the amplitude of the synthesized ground motions at 051JZW is smaller than that of the observed ground motions. It corresponds to the smaller amplitude of Fourier spectra or pseudo-velocity response spectrum of the synthesized ground motions in the range of 0.2s~1.0s. In contrast, the amplitude of the synthesized acceleration is larger than that of the observed acceleration at 051JZY, which might be related to the overestimation of high frequencies around 10.0Hz as shown in Fig. 5 and Fig. 6.

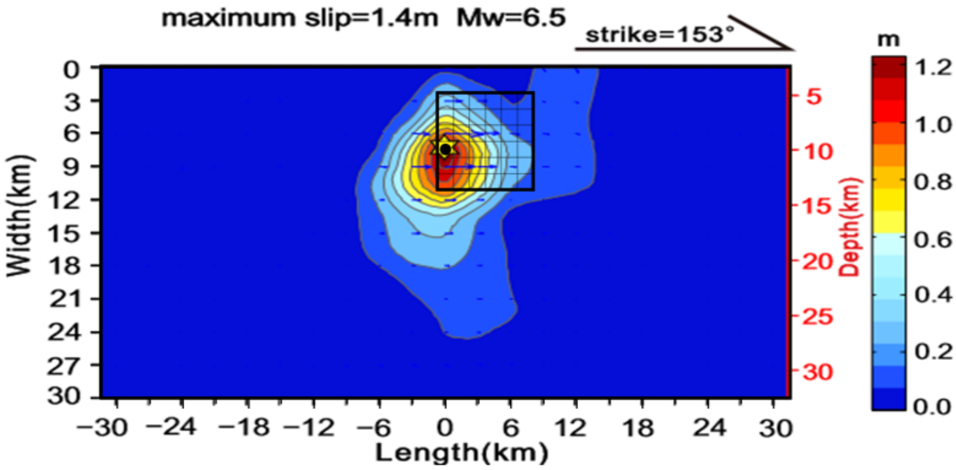

Fig. 3 – Layout of SMGA on the fault plane. The slip distributions are the results of [10].

Next, we examine the reasonability of the source parameters of the characterized source model. Somerville et al. [25] studied the scaling relationship that the combined area of asperities was linearly related with the seismic moment for crustal earthquakes as shown in the left panel of Fig. 7. Dan et al. [26] found that the amplitude of acceleration source spectra in the short period range was linearly related with the seismic moment as shown in the right panel of Fig. 7. The SMGA of the characterized source model is 8.76km in length and width, so it has an area of 76.7km^2, while the amplitude of acceleration source spectrum in the short period range of the characterized source model is 1.2×10^{19}N·m/s^2 which is evaluated from the radius of a circular fault whose area equals to the SMGA, stress parameter and S-wave velocity in the source region. These two parameters are shown with stars in the left and right panels, respectively, in Fig. 7. We also add the data evaluated from the results of the characterized source model for the southern fault segment during the 2008 M_w7.9 Wenchuan earthquake [27] and the characterized source model of the 2014

M_w6.1 Ludian earthquake [28], as shown with squares and diamonds, respectively, in Fig. 7. It should be noted that [27] construct the SMGAs only in the southern fault segment for the 2008 Wenchuan earthquake, thus the SMGAs and the seismic moment in the southern fault segment are shown in Fig. 7. We find that the SMGAs and the amplitudes of acceleration source spectra in the short period range for these three crustal earthquakes relate well with the corresponding seismic moments. Although the results for these three earthquakes with different magnitudes are still not enough, it suggests that the conventional scaling relationships developed by [25] and [26] could be used for prediction of ground motions in the future crustal earthquakes in China.

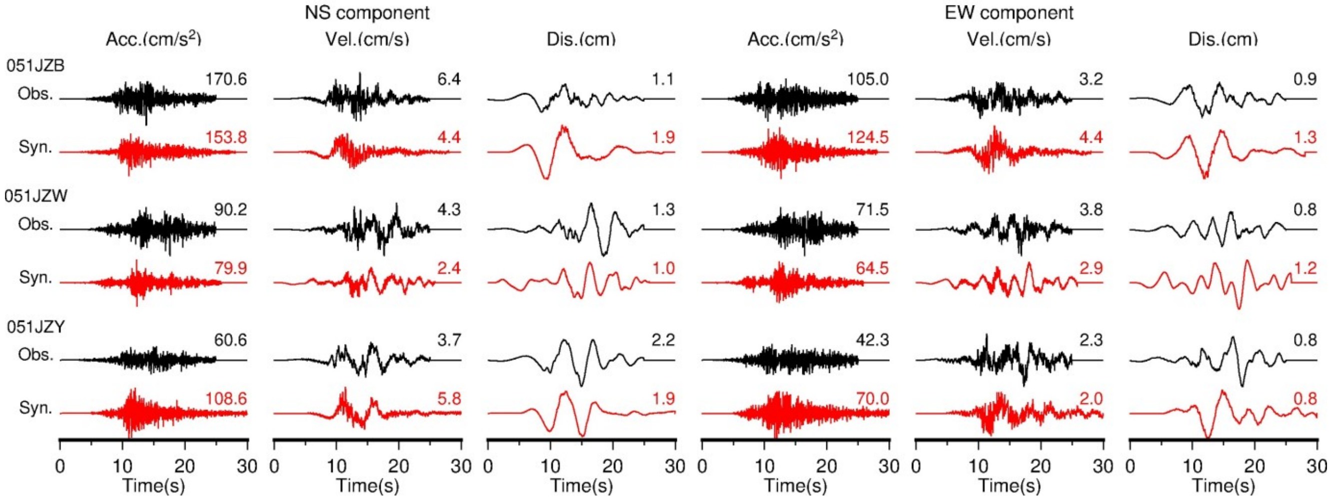

Fig. 4 – Comparison between observed (black) and synthesized (red) waveforms (acceleration, velocity and displacement) in the NS and EW components. The numerical values in the right top of waveforms are the peak values.

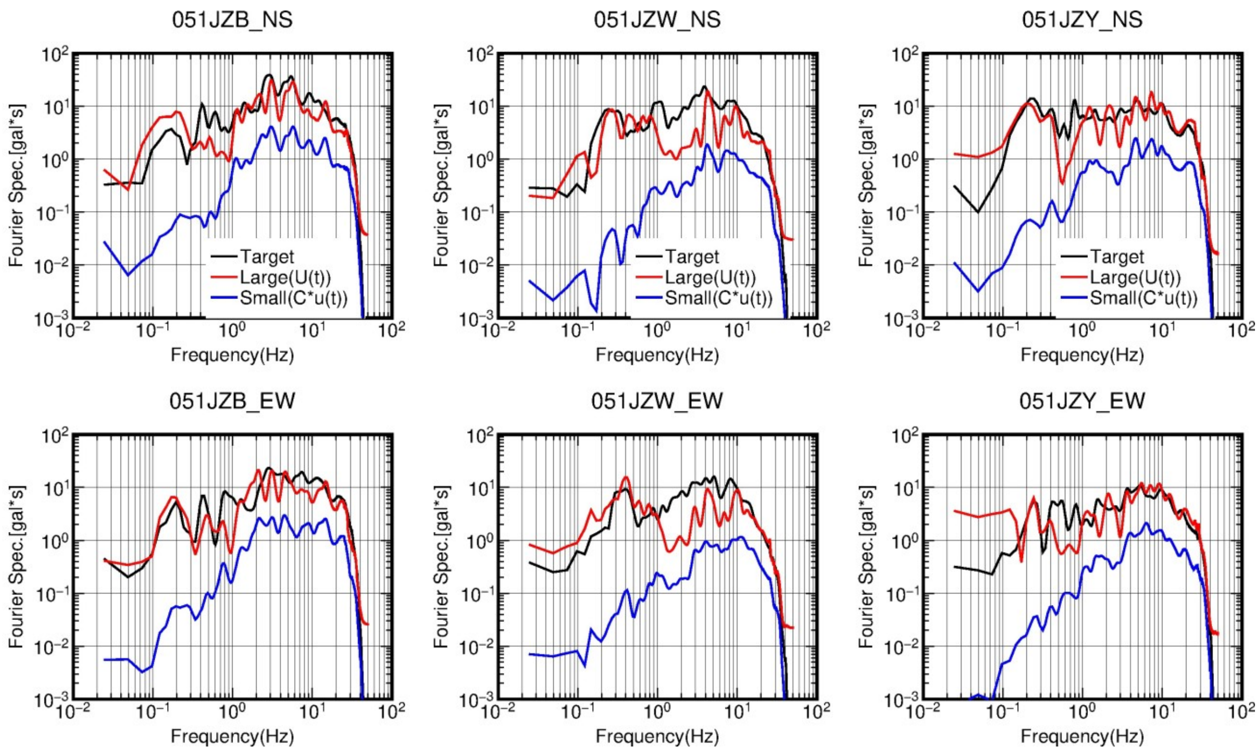

Fig. 5 – Comparisons of Fourier spectra between the synthesized and observed ground motions. The Fourier spectra are smoothed in the logarithm scale.

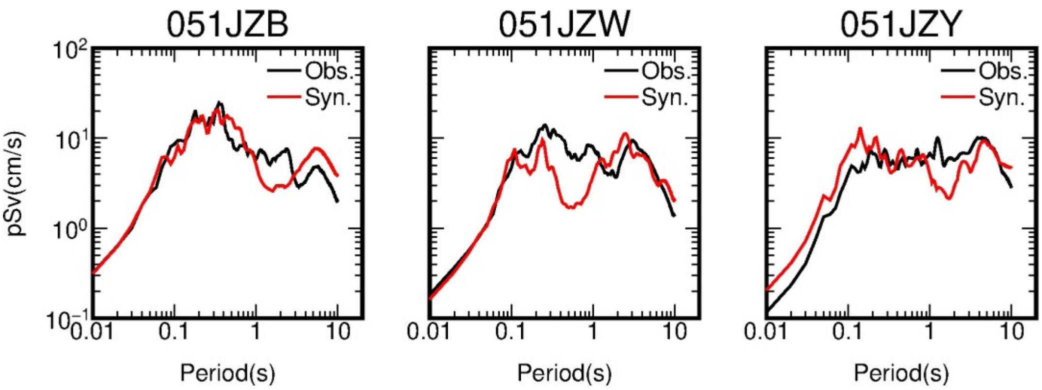

Fig. 6 – Comparisons of pseudo-velocity response spectra (damping ratio h=0.5%) between the synthesized and observed ground motions of the mainshock.

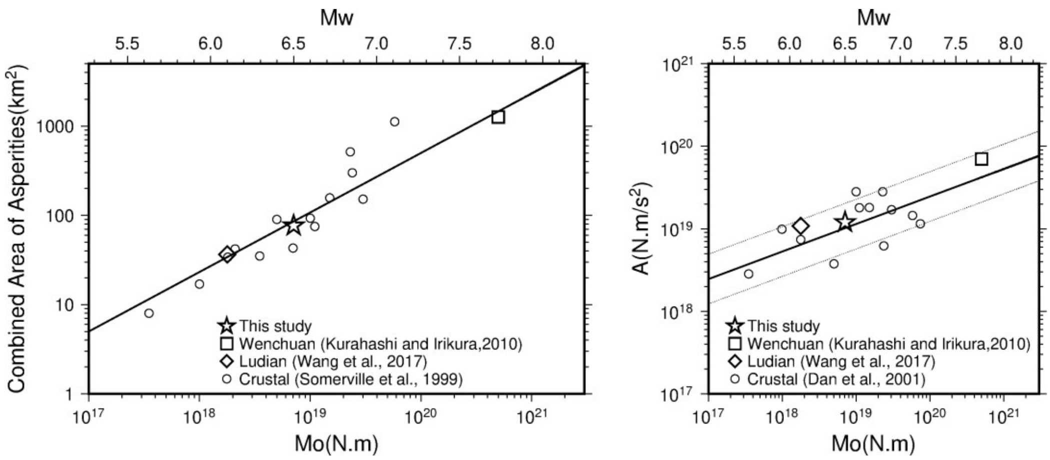

Fig. 7 – Conventional scaling relationship of combined area of asperities versus seismic moment [25] in the left panel, and conventional scaling relationship of acceleration source spectrum at short periods versus seismic moment [26] in the right panel. It should be noted that the SMGAs and the seismic moment in the southern fault segment rather than the entire fault model are used for the 2008 M_w7.9 Wenchuan earthquake [27].

5. Conclusions

The 2017 M_w6.5 Jiuzhaigou earthquake ruptured an unknown blind fault which might be the northern extension of Huya fault. It is essential to study the source model of this fault for prediction of ground motions in the future crustal earthquakes. We construct the characterized source model consisting of one SMGA inside the mainshock fault plane during the 2017 M_w6.5 Jiuzhaigou earthquake by use of the empirical Green's function method. We regard the ground motions of an M_w4.7 aftershock observed at three near-source strong-motion stations (i.e. 051JZB, 051JZW, and 051JZY) to be the EGFs of which the hypocenter is near the large slips areas of the mainshock and the source mechanism is similar to the mainshock. We estimate the fault size of the EGF event (1.46km in length and width) by the source spectral ratio method, and determine other parameters by simulated annealing algorithm, including the proportion coefficients C=1.54 and N=6, rupture velocity V_r=2.7km/s, rise time of the mainshock T=0.6s, and the indices of the rupture starting point (1,4). The area, stress parameter and seismic moment of the SMGA are 76.7km^2, 16.8MPa and 4.6×10^{18}N·m, respectively. We confirm that the characterized source model is capable of synthesizing the ground motions in the period range of 0.05s~5.0s within the engineering interests, as the synthesized ground motions are in reasonably good agreement with the observed ground motions at three strong-motion stations, both in waveforms and in pseudo-velocity response spectra. We find that the relationships between the SMGA and the seismic moment and between the amplitude of acceleration source spectrum in the short period range and the seismic moment for the 2017 M_w6.5 Jiuzhaigou earthquake, the 2013 M_w6.1 Ludian earthquake, and the 2008 M_w7.9 Wenchuan earthquake agree well with the conventional scaling relationships developed by [25] and [26]. It suggests that those conventional scaling relationships are applicable for the prediction of ground motions in the future crustal earthquakes in China.

6. References

[1] Li H, Liu JL, Jiang XL, Lv GJ, Li J (2013): Characteristic hazard analysis of the Jiuzhaigou M_s7.0 earthquake in 2017. *Technology for Earthquake Disaster Prevention* 13(3): 679-688 (in Chinese with English abstract)

[2] Wang J, Jin W, Cui YF, Zhang WF, Wu CH, Pasuto A (2018): Earthquake-triggered landslides affecting a UNESCO Natural Site: the 2017 Jiuzhaigou earthquake in the World National Park, China. *J. Mt. Sci.* 15(7): 1412-1428.

[3] Han LB, Cheng J, An YR, Fang LH, Jiang CS, Chen B, Wu ZL, Liu J, Xu XW, Liu RF, Yao ZX, Wang CZ, Wang YS (2018): Preliminary report on the 8 August 2017 M_s7.0 Jiuzhaigou, Sichuan, China, earthquake. *Seismol Res Lett* 89(2A): 557-569

[4] Fan XM, Scaringi G, Xu Q, Zhan WW, Dai LX, Li YS, Pei XJ, Yang Q, Huang RQ (2018): Coseismic landslides triggered by the 8th August 2017 M_s7.0 Jiuzhaigou earthquake (Sichuan, China): factors controlling their spatial distribution and implications for the seismogenic blind fault identification. *Landslides* 15: 967-983

[5] Sun JB, Yue H, Shen Z, Fang L, Zhan Y, Sun X (2018): The 2017 Jiuzhaigou earthquake: A complicated event occurred in a young fault system. *Geophysical Research Letter* 45.

[6] Nie ZS, Wang DJ, Jia ZG, Yu PF, Li LF (2018): Fault model of the 2017 Jiuzhaigou M_w6.5 earthquake estimated from coseismic deformation observed using Global Positioning System and Interferometric Synthetic Aperture Radar data. *Earth, Planets and Space* 70: 55

[7] Shan B, Zheng Y, Liu CL, Xie ZJ, Kong J (2017): Coseismic Coulomb failure stress changes caused by the 2017 *M*7.0 Jiuzhaigou earthquake, and its relationship with the 2018 Wenchuan earthquake. *Science China Earth Sciences* 60: 2181-2189

[8] Xie ZJ, Zheng Y, Yao HJ, Fang LH, Zhang Y, Liu CL, Wang MM, Shan B, Zhang HP, Ren JJ, Ji LY, Song MQ (2018): Preliminary analysis on the source properties and seismogenic rupture of the 2017 M_s7.0 Jiuzhaigou earthquake. *Science China Earth Sciences* 61: 339-352

[9] Zhang X, Feng WP, Xu LS, Li CL (2017) The source-process inversion and the intensity estimation of the 2017 M_s7.0 Jiuzhaigou earthquake. *Chinese J. Geophys.* 60(10): 4105-4116 (in Chinese with English abstract)

[10] Li Q, Tan K, Wang DZ, Zhao B, Zhang R, Li Y, Qi YJ (2018): Joint inversion of GNSS and teleseismic data for the rupture process of the 2017 M_w6.5 Jiuzhaigou, China, earthquake. *J Seismol* 22: 805-814

[11] Sun JZ, Yu YY, Li YQ (2018) Stochastic finite-fault simulation of the 2017 Jiuzhaigou earthquake in China. *Earth, Planets and Space* 70: 128

[12] Hartzell SH (1978): Earthquake aftershocks as Green's functions. *Geophys Res Lett* 5: 1-4

[13] Kanamori H (1979): A semi-empirical approach to prediction of long-period ground motions from great earthquakes. *Bull Seismol Soc Am* 69: 1645-1670

[14] Irikura K (1983): Semi-empirical estimation of strong ground motions during large earthquakes. *Bull Disas Prev Res Inst*, Kyoto University, 33: 63-104

[15] Irikura K (1986): Prediction of strong acceleration motions using empirical Green's function. *Proc 7th Japan earthquake engineering symposium*, Tokyo: 151-156

[16] Irikura K, Kagawa T, Sekiguchi H (1997): Revision of the empirical Green's function method by Irikura (1986). *Programme and abstracts of the Seismological Society of Japan*, 2 (in Japanese)

[17] Deng QD, Zhang P, Ran Y, Yang X, Min W, Chu Q (2003): Basic characteristics of active tectonics of China. *Science in China (Series D)* 46(4): 356-372

[18] Yi GX, Long F, Liang MJ, et al. (2017): Focal mechanism solutions and seismogenic structure of the 8 August 2017 Jiuzhaigou earthquake and its aftershocks. *Chinese Journal of Geophysics 60*(10): 4083-4097 (in Chinese with English abstract)

[19] Miyake H, Iwata T, Irikura K (2003): Source characterization for broadband ground-motion simulation: kinematic heterogeneous source model and strong motion generation area. *Bull Seismol Soc Am* 93(6): 2531-2545

[20] Zhang Y, Wang RJ, Chen YT, Xu LS, Du F, Jin MP, Tu HW, Dahm T (2014): Kinematic rupture model and hypocenter relocation of the 2013 M_w6.6 Lushan earthquake constrained by strong-motion and teleseismic data. *Seismol Res Lett* 85(1): 15-22

[21] Brune JN (1970): Tectonic stress and spectra of seismic shear waves from earthquakes. *J Geophys Res* 75: 4997-5009

[22] Brune JN (1971): Correction. *J Geophys Res* 76: 5002

[23] Eshelby JD (1957): The determination of the elastic field of an ellipsoidal inclusion and related problems. *Proc. Roy. Soc. London, Series A*, 241: 376-396

[24] Satoh T (2006): Inversion of Qs of deep sediments from surface-to-borehole spectral ratios considering obliquely incident SH and SV waves. *Bull Seismol Soc Am* 96(3): 943-956

[25] Somerville P, Irikura K, Graves R, Sawada S, Wald D, Abrahamson N, Iwasaki Y, Kagawa T, Smith N, Kowada A (1999): Characterizing crustal earthquake slip models for the prediction of strong ground motion. *Seismol Res Lett* 70: 199-222

[26] Dan K, Watanabe M, Sato T, Ishi T (2001): Short-period source spectra inferred from variable-slip rupture models and modeling of earthquake faults for strong motion prediction by semi-empirical method. *J Struct Const Eng, Architecture Institute of Japan* 545: 51-62 (in Japanese with English abstract)

[27] Kurahashi S and Irikura K (2010): Characterized source model for simulating strong ground motions during the 2008 Wenchuan earthquake. *Bull Seismol Soc Am* 100(5B): 2450-2475

[28] Wang X, Kurahashi S, Wu H, Si HJ, Ma Q, Dang J, Tao DW, Feng JW, Irikura K (2017): Building damage concentrated in Longtoushan town during the 2014 M_s6.5 Ludian earthquake, Yunan, China: examination of cause and implications based on ground motion and vulnerability analyses. *J Seismol* 21(5): 1185-1200

